

The Red Giant Branch in Near-Infrared Colour-Magnitude Diagrams. I: The calibration of photometric indices ^{*}

E. Valenti^{1,2}, F. R. Ferraro¹, L. Origlia²

¹ *Dipartimento Astronomia, Università di Bologna, Via Ranzani 1, I-40127 Bologna, Italy, e-mail elena.valenti2@studio.unibo.it, ferraro@bo.astro.it*

² *INAF-Osservatorio Astronomico di Bologna, Via Ranzani 1, I-40127 Bologna, Italy, e-mail origlia@bo.astro.it*

19 May 2019

ABSTRACT

We present new high-quality near-infrared photometry of 10 Galactic Globular Clusters spanning a wide metallicity range ($-2.12 \leq [\text{Fe}/\text{H}] \leq -0.49$): five clusters belong to the Halo (namely, NGC 288, NGC 362, NGC 6752, M 15 and M 30) and five (namely, NGC 6342, NGC 6380, NGC 6440, NGC 6441 and NGC 6624) to the Bulge. By combining J, H and K observations with optical data, we constructed Colour-Magnitude Diagrams in various planes ((K,J-K), (K,V-K), (H,J-H), and (H,V-H)). A set of photometric indices (colours, magnitudes and slopes) describing the location and the morphology of the Red Giant Branch (RGB) have been measured. We have combined this new data set with those already published by Ferraro et al. (2000) and Valenti et al. (2004), and here we present an updated calibration of the various RGB indices in the 2MASS photometric system, in terms of the cluster metallicity.

Key words: Stars: evolution — Stars: C - M — Infrared: stars — Stars: Population II Globular Clusters: individual: (NGC 288, NGC 362, NGC 6752, M 15, M 30, NGC 6342, NGC 6380, NGC 6440, NGC 6441, NGC 6624) — techniques: photometric

1 INTRODUCTION

The study of stellar evolutionary sequences finds several applications in astrophysics: inferring the age and metallicity of stellar systems, synthesizing integrated spectra of galaxies, calibrating standard candles for distance determinations. There is a small number of physical observables that models can predict and that can be compared with observed quantities. Within this framework, Colour-Magnitude Diagram (CMD) and Luminosity Function (LF) are the most powerful tools to test theoretical models, being related to the stellar effective temperature, luminosity and the duration of a specific evolutionary phase (Renzini & Fusi Pecci 1988). In this contest, our group started a long-term project devoted to analyzing and testing each individual evolutionary sequence in the CMD of Galactic Globular Clusters (GGCs) (see e.g. Ferraro et al. 1999, 2000, hereafter F99 and F00, respectively). In particular, CMDs and LFs in the near-Infrared (IR) are useful in order to perform a detailed study of the Red Giant Branch (RGB). In fact, in study-

ing cool stellar populations (i.e. RGB stars), the near-IR spectral domain offers several advantages, being the most sensitive to low temperature. Moreover, the background contamination by Main Sequence (MS) stars is much less severe, thus allowing to properly characterize the RGB even in the innermost core region of stellar clusters affected by crowding. In addition, with respect to the visual range, in the IR range the reddening is much lower and in some cases, when the extinction is very large, as in the Bulge, it represents the only possibility to observe the stellar population along the entire RGB. This is well known since two decades, and several authors have used IR photometry to derive the main RGB properties (see e.g. F00 and references therein).

By combining near-IR and optical photometry one can also calibrate a few major indices with a wide spectral baseline, like for example the (V-K) colour, which turns out to be very sensitive to the stellar temperature. In this framework, F00, Valenti et al. (2004, -hereafter V04) and Sollima et al. (2004, -hereafter S04) presented near-IR CMDs of a total sample of 16 GGCs (10 in F00, 5 in V04 and 1 in S04) which have been used to calibrate several observables describing the RGB physical and chemical properties, and to detect the major RGB evolutionary features (i.e. the Bump and the Tip).

^{*} Based on data taken at the ESO-MPI 2.2m Telescope equipped with the near-IR camera IRAC2-ESO, La Silla (Chile), within the observing program 59.E-0340.

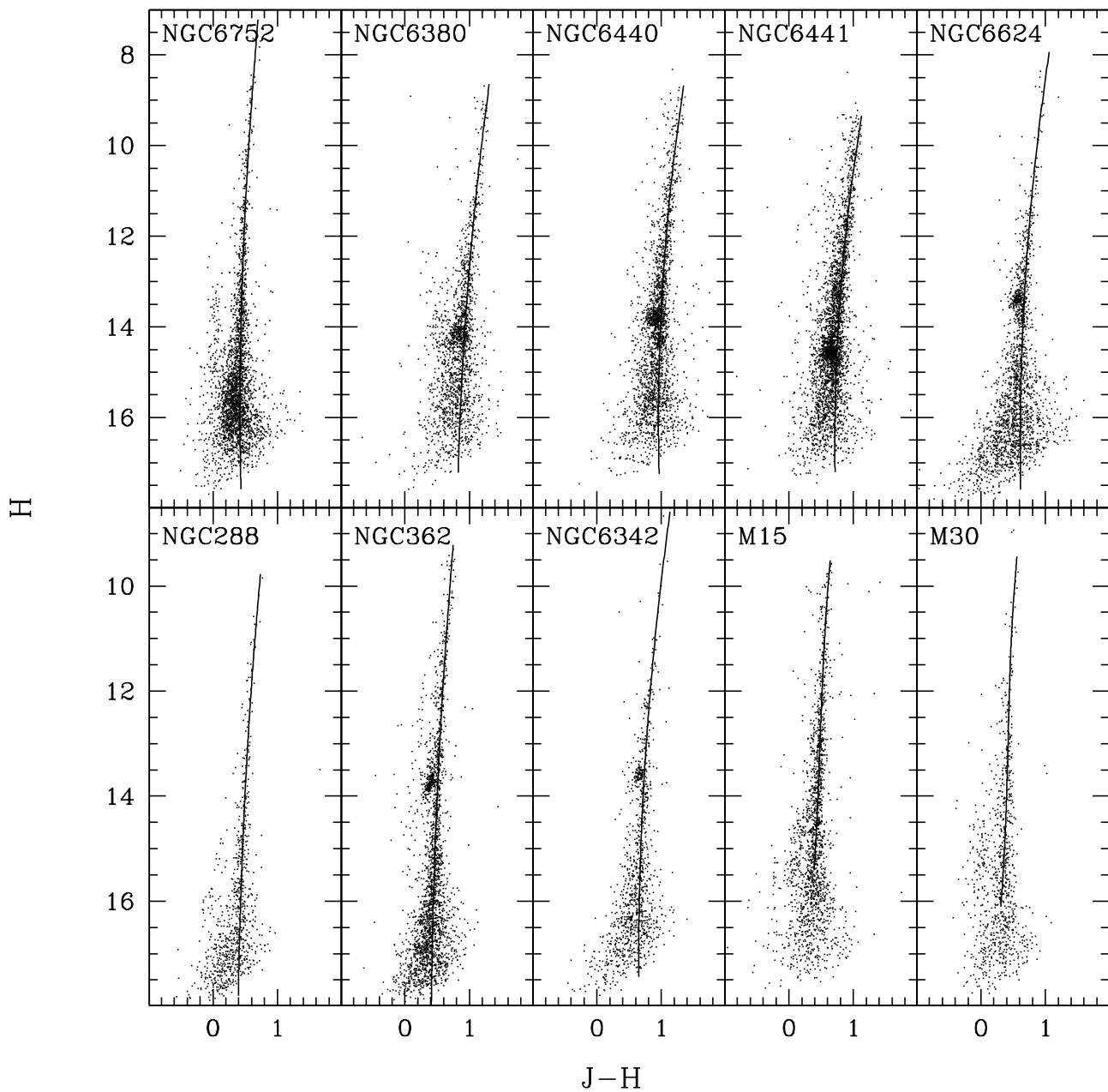


Figure 1. H, J-H colour-magnitude diagrams for the 10 GGCs in our database. The thick line in each panel indicates the RGB fiducial ridge line.

In this paper we present an additional sample of 10 clusters belonging to different Galactic populations: five clusters (namely NGC 288, NGC 362, NGC 6752, M 15 and M 30) belong to the Halo and five (namely NGC 6342, NGC 6380, NGC 6441, NGC 6440 and NGC 6624) belong to the Bulge. By combining the data set presented here and the data by F00, V04 and S04 we have now available a homogeneous near-IR database of 24 GGCs distributed over a wide metallicity range, $-2.12 \leq [\text{Fe}/\text{H}] \leq -0.49$. In this first paper we presented the new data set and the calibration of the various RGB photometric parameters (colours at fixed

magnitudes, magnitudes at fixed colours, slope) as a function of the cluster metallicity. This work represents an update of the calibrations presented by F00, based on a significant larger sample (especially in the high metallicity domain). Moreover, since H-band observations were also available we derive new calibrations of the RGB photometric indices in this band as well, in order to have a more complete set of metallicity tracers in the near-IR bands.

A forthcoming paper (Valenti, Ferraro & Origlia 2004, in preparation) will be devoted to discuss the major evolutionary features (bump and tip) and their calibration as

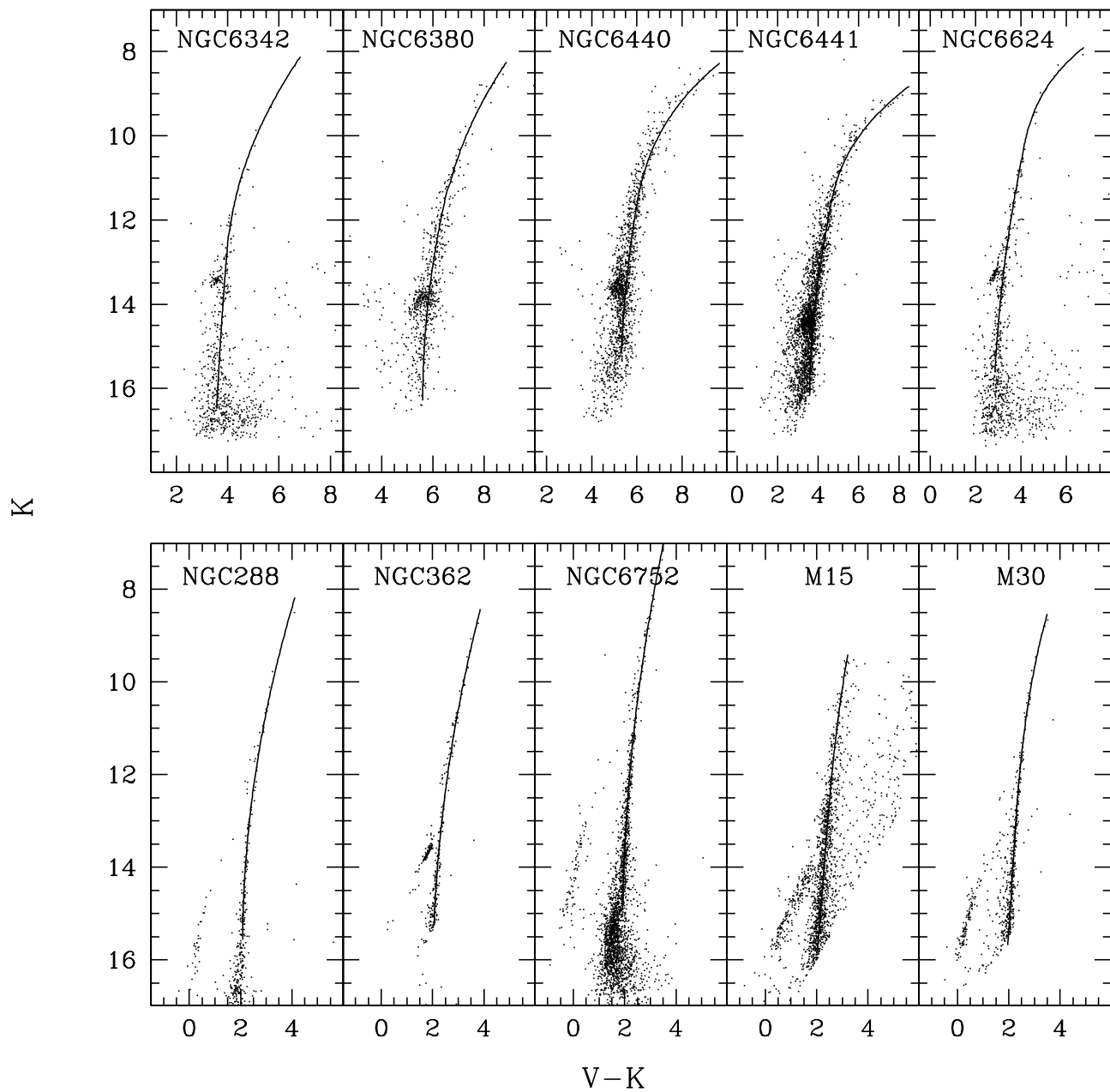


Figure 2. K, V-K colour-magnitude diagrams for the 10 GGCs in our database. The thick line in each panel indicates the RGB fiducial ridge line.

a function of the metallicity. A third paper (Ferraro et al. 2004, in preparation) will deal with the transformation to the theoretical plane and the definition of useful relation to empirically calibrate the mixing-length parameter of theoretical models.

The observations and data reduction are presented in §2, while §3 describes the properties of the observed CMDs. §4 is devoted to derive the mean RGB features from the CMDs and the comparison with the previous works. Finally, our conclusions are summarized in §5.

2 OBSERVATIONS AND DATA REDUCTION

A set of J, H and K images were secured at ESO, La Silla in August 1997, using the ESO-MPI 2.2m telescope equipped with the near-IR camera IRAC-2 (Moorwood et al. 1992) based on a NICMOS-3 256×256 array detector. The central 4′×4′ region of ten GGCs, namely NGC 288, NGC 362, NGC 6752, M 15, M 30, NGC 6342, NGC 6380, NGC 6440, NGC 6441 and NGC 6624, were mapped by using two different magnification: 0.28″/px for the most crowded central field and 0.51″/px for the four fields centred at ∼1′

Table 1. The observed sample

Name	$[Fe/H]_{CG97}$	Optical Photometry
<i>Halo Clusters</i>		
M 15	-2.12	Buonanno et al. (1985)
M 30	-1.91	Bergbusch (1996)
NGC 6752	-1.42	Ferraro et al. (2003)
NGC 362	-1.15	Bellazzini et al. (2001a)
NGC 288	-1.07	Bellazzini et al. (2001a)
47 Tuc	-0.70	Montegriffo et al. (1995)
<i>Bulge Clusters</i>		
NGC 6380	-0.87	Ortolani et al. (1998)
NGC 6342	-0.71	Piotto et al. (2002)
NGC 6441	-0.68	Piotto et al. (2002)
NGC 6624	-0.63	Piotto et al. (2002)
NGC 6440	-0.49	Ortolani et al. (1994)

north-east, north-west, south-east and south-west of the cluster centre. An additional cluster, 47 Tuc, was also observed, but only in the H band. Table 1 lists the observed clusters and their metallicity in the Carretta & Gratton (1997-hereafter CG97) scale.

During the four observing nights the average seeing was $1''$ - $1.2''$. Each J, H and K image was the resulting average of 60 exposures of 1-s detector integration time (DIT) and was sky-subtract and flat-field-corrected. The sky field was located several arcmin away from the cluster centre. More details on the pre-reduction procedure can be found in Ferraro et al. (1994) and Montegriffo et al. (1995). The Point Spread Function (PSF) fitting procedure was performed independently on each J, H and K image by using the ALLSTAR routine (Stetson & Harris 1988) of the reduction package DAOPHOTII (Stetson 1994). A catalog listing the instrumental J, H and K magnitudes for all the stars identified in each field has been obtained by cross-correlating the single band catalogs. All stars measured in at least two bands have been included in the final catalog. Since the observations were performed under not perfect photometric conditions, we transformed the instrumental magnitudes into the *Two Micron All Sky Survey* (2MASS) photometric system¹. The large number of stars (typically a few hundreds) in the overlapping area between our observation and 2MASS survey were used to derive the calibration to the 2MASS photometric system; only zero-order polynomial relations, without colour terms, have been used.

Since M 15 and M 30 were observed also by F00, their photometric catalogs were combined with ours in order to reduce the photometric uncertainties. First, the catalog of M 15 and M 30 by F00 were transformed in the 2MASS photometric system by using the empirical transformations

found by V04, then for each cluster we derived a unique catalog by averaging the multiple measurements.

An overall uncertainty of ± 0.05 mag in the zero point calibration in all the three bands, has been estimated. Fig. 1 and 2 show the H, J-H and K, V-K CMDs, respectively, for the observed clusters in the 2MASS system.²

3 COLOUR MAGNITUDE DIAGRAMS

More than 16,000 and 9,000 stars are plotted in the (H,J-H) and (K,V-K) CMDs shown in Figs. 1 and 2, respectively. The references for the optical data used in this work are listed in Table 1. The main characteristic of the CMDs are schematically summarized as follows:

i) The RGB is quite well populated in all the program clusters, even in the brightest magnitude bin, and allows us a clean definition of the mean ridge line, up to the end of the RGB.

ii) The observations are deep enough to detect the base of the RGB at $\Delta K \sim \Delta H \sim 7 - 8$ mag fainter than the RGB tip, and ~ 3 -4 mag below the Horizontal Branch (HB).

iii) In the combined CMDs the HB stars are clearly separable from the RGB stars. For the Halo cluster sample, the HB has an almost vertical structure in all the CMDs, as expected for a metal-poor population. The Bulge clusters exhibit a red clumpy HB, which is typical of metal-rich populations. In the case of NGC 6441, from the combined CMD it is possible to clearly see the anomalous HB which exhibits both the typical features of metal-poor and metal-rich populations, a red clump and a populated blue branch (see also Rich et al. 1997).

3.1 Comparison with previous photometries

Some of the program clusters, mainly those belonging to the Halo, have been the subject of several photometric and spectroscopic observations in the optical bands. For example, NGC 288 and NGC 362, represent an HB *Second Parameter pair* (see Bellazzini et al. 2001a, and references therein), and NGC 6441 has been observed by several authors for its peculiar HB morphology (see Rich et al. 1997, and references therein). However, only a few papers presented IR photometry for the clusters in our sample. Frogel et al. (1983b) reported J, H and K photometry of giants in NGC 288, NGC 362 and NGC 6752. A direct star-to-star comparison was not possible because the authors did not published the coordinates of the observed stars; nevertheless their photometries nicely overlap our IR-CMDs with a minor offset of $\approx (0.03 - 0.05)$ mag. The comparison of our K, J-K CMD of NGC 288 with the mean ridge line published by Davidge & Harris (1997) shows a good agreement. For M 15 and M 30 a comparison with previous photometries can be found in F00.

Conversely, for NGC 6440 and NGC 6624 a star-to-star comparison between our data and the J, H and K photometry published by Kuchinski & Frogel (1995) is possible. They

¹ In doing this we used the Second Incremental Release Point Source Catalog of 2MASS

² The observed cluster catalogs, in the 2MASS photometric system are available in the electronic form.

Table 2. Reddening estimates for the program Bulge clusters.

Cluster	[Fe/H] _{CG97}	E(B-V) _{Harris96}	E(B-V) _{Schlegel98}	E(B-V) _{derived}	E(B-V) _{adopted}
NGC 6342	-0.71	0.46	0.57	0.56	0.57
NGC 6380	-0.87	1.17	1.52	1.29	1.29
NGC 6441	-0.68	0.44	0.63	0.52	0.52
NGC 6624	-0.63	0.28	0.14	0.34	0.28
NGC 6440	-0.49	1.07	1.15	1.17	1.15

mapped a field of $2.5' \times 2.5'$ centred $\sim 1'$ north-east from the centre in both clusters, using a $0.35''/px$ magnification. An offset of ≈ 0.15 mag was found in all the three bands. Also Minniti et al. (1995) presented IR- photometry of NGC 6440, but no online data are available, however their data agree with Kuchinski & Frogel (1995). Though the 2MASS photometric system is different from that used by Kuchinski & Frogel (1995) the measured offset seems too large to be due only to the different photometric systems. IR photometric studies of NGC 6342 and NGC 6380 are not available in the literature.

4 THE MAIN RGB FEATURES

The main aim of this series of papers is to present updated calibrations of photometric RGB indices as a function of the metallicity, based on a complete database collected by our group over the last 10 years, and presented in F00, V04 and this paper. In this section the RGB ridge lines and a few major photometric indices, namely colours at fixed magnitudes and magnitudes at fixed colours accordingly to the definitions by F00, are derived from the CMDs shown in Fig. 1 and 2. In order to properly combine this data set with those by F00 and V04, we first need to make homogeneous the photometric systems. In particular, we converted the photometry presented in F00 and V04 in the 2MASS system by using the relation found by V04. In the case of ω Cen, the RGB ridge line was converted in the 2MASS photometric system by using the offset found by S04 ($\Delta J=0.0$ and $\Delta K=-0.04$). After this transformation, a homogeneous data set of 24 clusters is available. The RGB ridge lines and the photometric indices of the entire sample have been newly determined. Of course all the known RGB variables lying in the region sampled by our observations (see the case of 47 Tuc and NGC 6553 in Figs. 1 and 2 of F00) have been identified and removed from the RGB sample before measuring any parameter.

4.1 The RGB fiducial ridge lines

Since the procedure to obtain the RGB fiducial ridge lines for the observed clusters has been fully described in F00 and V04, it will not be repeated here. The ridge lines for the 10 clusters presented here are overplotted to the (H,J-H) and (K,V-K) CMDs shown in Fig. 1 and 2, respectively.

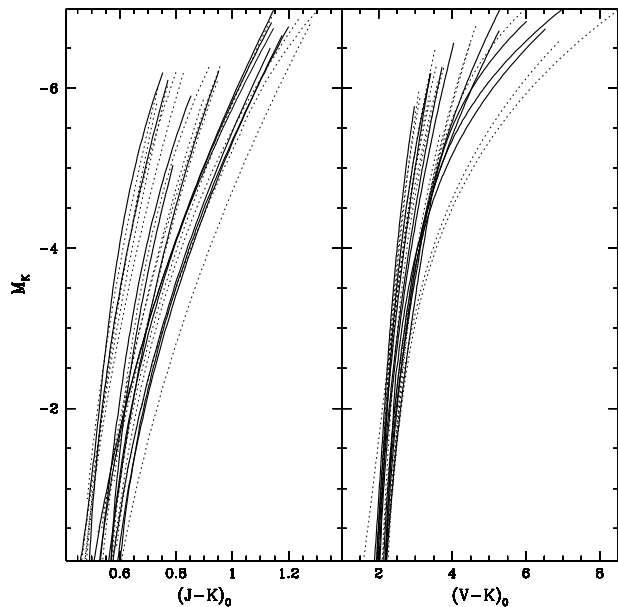


Figure 3. RGB fiducial ridge lines for the observed GCGs (solid lines) in the $M_K, (J-K)_0$ (left panel) and $M_K, (V-K)_0$ (right panel). The mean ridge lines for the clusters presented by F00, V04 and S04 (transformed in the 2MASS photometric system) are plotted as dotted lines.

4.2 Reddening and distance modulus

In order to transform the mean ridge lines into the absolute plane it is necessary to adopt a distance scale and a reddening correction. The definition of the most suitable distance scale for GCGs is still very controversial (see F99 and references therein). In the present study, the distance scale established by F99 was adopted. Nevertheless, in the F99 clusters list (see their Table 2) only the Halo clusters sample are considered. For the Bulge clusters we derived an independent distance modulus from the IR photometry presented here. In doing this, we compared the IR and combined CMDs of the Bulge clusters with those of a *reference* cluster. This method allows, in principle, to derive simultaneously distance modulus and reddening estimates. In fact, the needed colour and magnitude shifts to overlap the CMDs of two clusters of comparable age and metallicity, are a function of the reddening and distance differ-

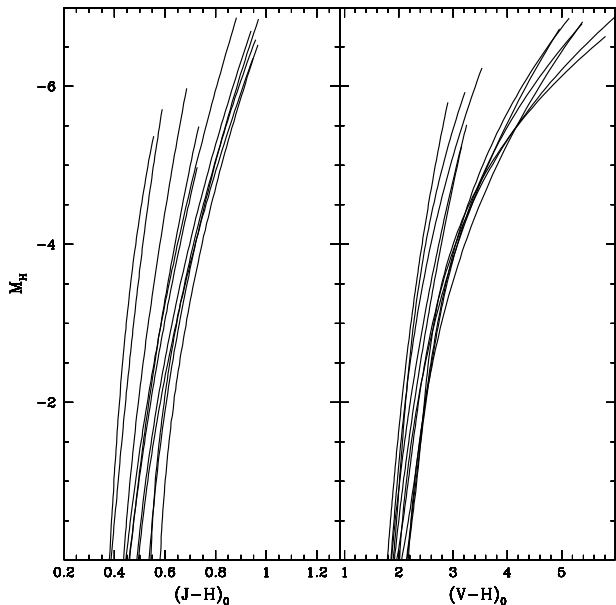


Figure 4. RGB fiducial ridge lines for the 10 observed GGCs and for 47 Tuc, in the $M_H, (J-H)_0$ (left panel) and $M_H, (V-H)_0$ (right panel).

Table 3. Adopted parameters for the observed GGCs.

Name	$[Fe/H]_{CG97}$	$[M/H]$	$E(B-V)$	$(m-M)_0$
<i>M</i> 15*	-2.12	-1.91	0.09	15.15
<i>M</i> 30*	-1.91	-1.71	0.03	14.71
<i>NGC</i> 6752*	-1.42	-1.21	0.04	13.18
<i>NGC</i> 362*	-1.15	-0.99	0.05	14.68
<i>NGC</i> 288*	-1.07	-0.85	0.03	14.73
<i>NGC</i> 6380	-0.87	-0.68	1.29	14.81
<i>NGC</i> 6342	-0.71	-0.53	0.57	14.63
<i>NGC</i> 6624	-0.63	-0.48	0.28	14.63
<i>NGC</i> 6441	-0.68	-0.52	0.52	15.65
<i>NGC</i> 6440	-0.49	-0.40	1.15	14.58
47 <i>Tuc</i> *	-0.70	-0.59	0.04	13.32

* For these clusters the estimates listed in Table 2 of F99 have been used.

ences, respectively. Since several works on dating the Bulge GCs have showed that Halo and Bulge GCs have comparable age (see i.e. Momany et al. 2003; Heasley et al. 2000; Feltzing & Johnson 2002; Ortolani et al. 2001), and since our Bulge cluster sample has a metallicity comparable to that of 47 Tuc (within 0.2 dex, see Table 1), we decided to adopt 47 Tuc as a reference cluster. Moreover, the reddening, the metallicity and the distance of 47 Tuc are reasonably known, being one of the most studied GGC since many decades. As can be seen from Table 2, also the reddening determination of the Bulge clusters is quite uncertain (compare the values listed by Harris (1996) with the most re-

cent determination by Schlegel et al. (1998)). Of course a different assumption on the reddening significantly affects the position of the RGB in the absolute plane and the determination of the true distance modulus. For this reason we used the differential analysis described above, in order to derive an independent reddening estimate and to decide the most appropriate reddening for each Bulge cluster in our sample. Of course, the position of the RGB in the CMD is a sensitive function of the metallicity, for this reason the differential method should be applied to clusters with similar metallicity. From the relations found by F00 we estimate that a difference of ≈ 0.2 dex in metallicity would produce a difference of ≈ 0.04 in the $(J-K)$ colour and ≈ 0.1 in $(V-K)$. As can be seen from Table 1, three Bulge clusters in our sample (namely, *NGC* 6342, *NGC* 6624 and *NGC* 6441) have a metallicity (in the CG97 scale) comparable to 47 Tuc (within 0.1 dex). *NGC* 6380 has a nominal metallicity 0.2 dex lower than 47 Tuc, but the well defined HB clump and the RGB shape suggest a higher metallicity, for this cluster. Previous papers (e.g. Ortolani et al. 1998) already suggested for *NGC* 6380 a metallicity between 47 Tuc and *NGC* 6553. Finally, *NGC* 6440 is ≈ 0.2 dex more metal-rich than the reference cluster. We applied the differential method to the Bulge clusters in our sample, and the shifts in colours in different planes (i.e. $\delta(J-H)$, $\delta(J-K)$, $\delta(V-J)$, $\delta(V-H)$, $\delta(V-K)$) have been computed. Then, by adopting extinction coefficient for the V, J, H and K band listed by Savage & Mathis (1979) ($A_V/E(B-V) = 3.1$, $A_J/E(B-V) = 0.87$, $A_H/E(B-V) = 0.54$ and $A_K/E(B-V) = 0.38$) we derived the average value for the reddening. The result of this procedure is shown in Table 2. As can be seen the value found by our procedure is similar to that found by Schlegel et al. (1998) for *NGC* 6440 and *NGC* 6342, while it is more similar to the Harris (1996) value for *NGC* 6624. For two clusters in our sample, namely *NGC* 6380 and *NGC* 6441, the reddening obtained by our procedure is significantly different (and intermediate) from both the literature values. For these two clusters we will adopt our reddening value. However, to be conservative, these two clusters are not considered in deriving the relations between the position in colour of the RGB and the clusters metallicity (in different planes). By assuming the reddening listed in column [6] of Table 2 we derived the distance modulus by comparison with 47 Tuc. The HB clump has been chosen as a reference sequence.

The adopted method can be summarized as follow:

- i*) The LFs in the IR passbands have been constructed to identifying the HB peak, which it is been used as HB level.
- ii*) By using the LFs we measured the differences between the 47 Tuc HB level and those of the Bulge clusters; the derived values have been adopted to shift the clusters CMD on the reference one.
- iii*) Finally, the differences in magnitudes measured in the various bands have been corrected for reddening (by using the relations quoted above) and the true distance modulus has been obtained.

It is worth noting that in applying this method, all the available photometric bands were used in order to get a more careful estimate. Table 3 lists the adopted distance modulus for all the program clusters.

Fig. 3 shows the observed RGB fiducial ridge lines in the absolute M_K , $(J-K)_0$ and M_K , $(V-K)_0$ planes for the entire database of 24 GGCs (the 10 clusters presented here

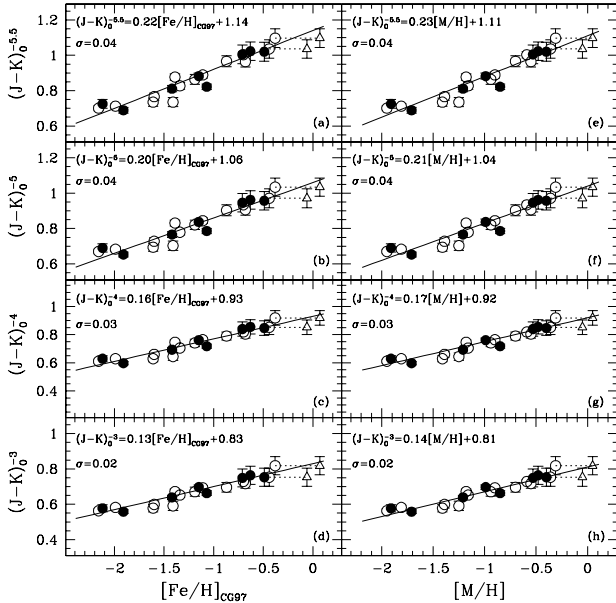


Figure 5. RGB mean $(J-K)_0$ colour at fixed ($M_K = -5.5, -5, -4, -3$) magnitudes as a function of the CG97 metallicity scale (left panels) and of the global metallicity (right panels). Filled circles: the 10 clusters observed here. Empty circles: the F00, V04 and S04 samples. The empty triangles refer to NGC 6553 and NGC 6528 adopting the Carretta et al. (2001) metallicity estimates. The solid lines are best-fitting relations.

are plotted as solid lines). As expected, the mean ridge lines of our 5 intermediate-low metallicity clusters lie in the bluer region of the diagrams, while in the redder part we find those of high-metallicity clusters of the Bulge. A similar behavior can be seen in Fig. 4, which shows the RGB ridge lines in the absolute M_H , $(J-H)_0$ and M_H , $(V-H)_0$ planes. In the M_H , $(V-H)_0$ plane, the two different groups are more clearly distinguished. The Halo cluster RGB lines are bluer and less curved than the RGB lines of the more metal-rich Bulge clusters.

4.3 The RGB location in Colour and in Magnitude

As already discussed in detail by F00, to properly characterize the overall behavior of the RGB as a function of the cluster metallicity, a set of photometric indices are needed (see §4). In fact, at fixed colours the corresponding magnitudes mark different RGB regions, depending on the clusters metallicity. Several parameters describing the RGB location in colour and in magnitude have been suggested by many authors (see F00 and references therein). Nevertheless, to get a complete description of the RGB photometric properties, in the present study we use the new parameters defined by F00, namely the $(J-K)_0$ and $(V-K)_0$ colours at different absolute magnitudes $M_K = -3, -4, -5, -5.5$, and the K absolute magnitude at fixed $(J-K)_0$ and $(V-K)_0$ colours, respectively. The derived $(J-K)_0$ and $(V-K)_0$ RGB colours for the program clusters are listed in Table 4 and 5, respectively. In both tables, the measurements by F00 and V04,

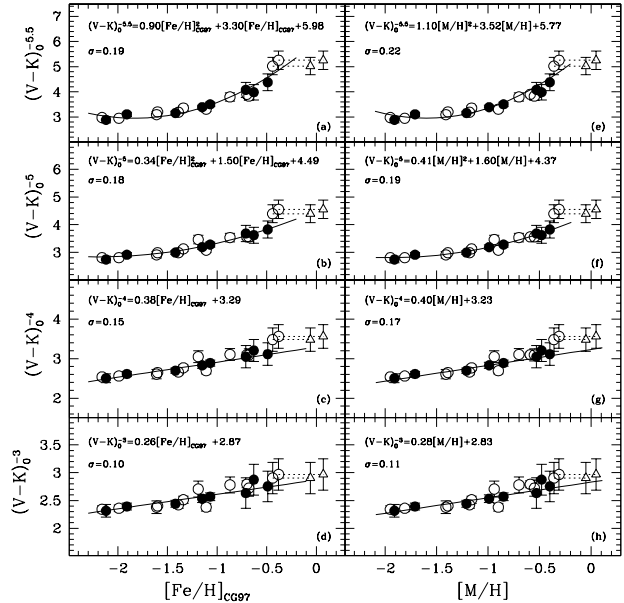


Figure 6. The same as Fig. 5, but for $(V-K)_0$ colours.

converted in the 2MASS photometric system, are also reported. The colours at fixed magnitudes for all the clusters in the database have been calibrated as a function of: *i*) the metallicity in the CG97 scale, and *ii*) the global metallicity ($[M/H]$) defined and computed in F99, which takes into account the contribution of the α -elements in the definition of the global metallicity of the cluster. The metallicity in the CG97 scale for the program clusters has been computed from the Zinn (1985) scale by using equation [7] of CG97, following the prescriptions by F99. The typical uncertainty on the derived metallicities can be conservatively assumed to be 0.2 dex; however, for clusters having direct CG97 measurements the error is significantly lower, <0.1 dex, (see Table [8] of CG97).

The calibration relations of the RGB photometric indices as function of the cluster metallicity in both the adopted scales are listed in the Appendix.

The case of NGC 6553 and NGC 6528 (the two clusters which represent the metal-rich extreme of our entire database) deserves a few additional comments. The metallicity of these two clusters has been, in fact, largely debated in the literature. By simply considering the most recent determinations based on high resolution spectroscopy, values ranging from -0.3 up to about solar (Carretta et al. 2001; Origlia et al. 2002; Melendez et al. 2003) have been proposed. To be homogeneous with other clusters, for NGC 6553 and NGC 6528 in the following calibrations we will adopt the CG97 values listed in Table 5. Figs. 5 and 6 show the $(J-K)_0$ and $(V-K)_0$ colours as a function of both the CG97 and global metallicity scales, for the entire sample of 24 clusters. By using the full data set, updated calibrations have been derived and reported in each panel and in the Appendix. As can be seen from Fig. 5 the RGB $(J-K)_0$ colours linearly scale with the metallicity. As expected from previous studies (see Cohen & Sleeper 1995, and F00) the fit slope increases progressively toward

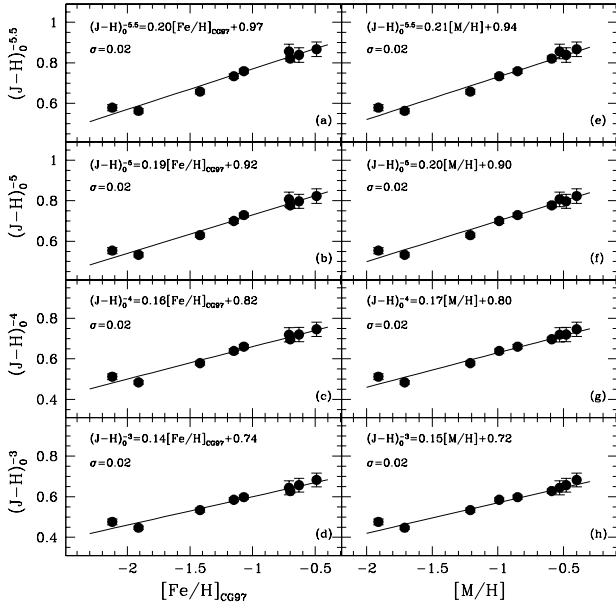


Figure 7. RGB mean $(J-H)_0$ colour at fixed ($M_H = -5.5, -5, -4, -3$) magnitudes as a function of the CG97 metallicity scale (left panels) and of the global metallicity (right panels) for the observed clusters. The solid lines are best-fitting relations.

the RGB tip. The derived slope values are consistent with those found by F00. Conversely, in the $(V-K)_0$ plane, the best-fitting solution deviates from a linear dependence at higher metallicity (see Fig. 6, panels *a, b, e, f*) even if the Carretta et al. (2001) metallicity estimates for the most metal-rich clusters are adopted. As can be seen the RGB, particularly near the tip, rapidly becomes redder and redder as the metallicity increases as shown by Cohen & Sleeper (1995) and successively confirmed by F00.

For NGC 6624, Cohen & Sleeper (1995) derived the $(J-K)_0$ and $(V-K)_0$ colours at fixed absolute magnitude $M_K = -4, -5$. Their estimates in the K, $(J-K)$ plane (see their Table 10) are systematically redder, by ~ 0.15 with respect to our determinations. This is due to different reddening and distance assumptions: when we apply their reddening and distance modulus values to our photometry, the difference in the derived $(J-K)_0$ colours is reduced to only ~ 0.03 mag. In the K, $(V-K)$ plane, a ~ 0.1 mag difference remains even when the same reddening and distance modulus are adopted. Conversely, a nice agreement in the derived $(V-K)_0^{M_K=-5}$ colour was found with the value published by Kuchinski & Frogel (1995).

By using $(J-H)_0$ and $(V-H)_0$ colours at different absolute magnitudes $M_H = (-3, -4, -5, -5.5)$, new calibrations have been proposed in the H band. The derived values for the program clusters are listed in Table 6 and 7, while Figs. 7 and 8 show the behavior of the $(J-H)_0$ and $(V-H)_0$ colours, respectively, as a function of the cluster metallicity in both the adopted metallicity scales. The best fits to the data are shown in each panel and listed in the Appendix. As expected, the colours become redder with increasing clusters metallicity in a linear way and independently from

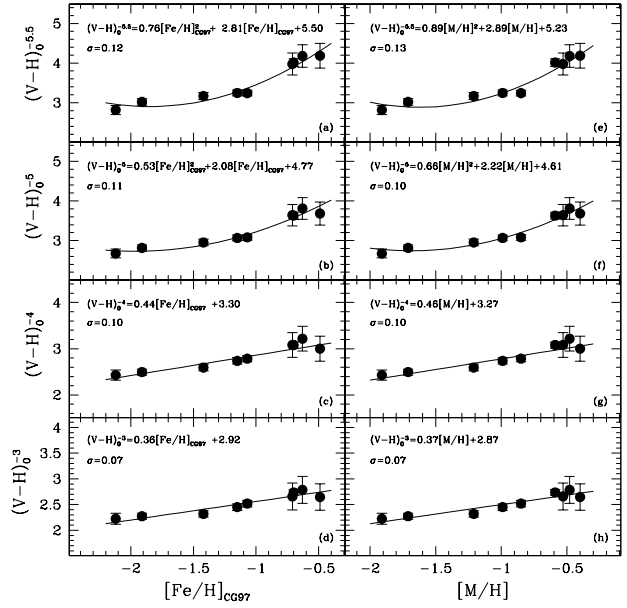


Figure 8. The same as Fig. 7, but for $(V-H)_0$ colours.

the height cut in the H, $(J-H)$ plane, while at brighter magnitudes the $(V-H)_0$ colour shows a quadratic metallicity dependence.

Following Frogel et al. (1983) and F00 we also measured the K absolute magnitude at fixed $(V-K)_0 = 3$ and $(J-K)_0 = 0.7$ colours. In Fig. 9 we show the dependence of these parameters on metallicity in both the adopted scales, for the entire sample. The best-fitting relations are also reported in each panel. Table 4 and 5 list the derived M_K magnitudes at constant $(J-K)_0$ and $(V-K)_0$ colours, respectively. While the error associated to the determination of the colours at fixed absolute magnitudes are mainly driven by the uncertainty on the distance modulus, the accuracy on the derived absolute magnitude at fixed colours depends on both distance and reddening uncertainties with almost the same weight. In fact, given the intrinsic steepness of the RGB, especially in the metal-poor range, an error of a few hundredths of magnitude in the reddening correction easily implies 0.15-0.20 mag uncertainty in the derived M_K absolute magnitudes, depending on the height along the RGB (see Fig. 3).

By using the same strategy we also derive the M_H absolute magnitude at fixed $(J-H)_0 = 0.7$ and $(V-H)_0 = 3$ colours, listed in Tables 6 and 7 and plotted in Fig. 10 as a function of the metallicity in both the adopted scales. The best-fitting relations with the corresponding standard deviation are reported in each panel and listed in the Appendix.

4.4 The RGB slope

An useful parameter to provide a photometric estimate of the cluster metallicity is the so-called RGB slope. This parameter turns to be extremely powerful since it is independent from reddening and distance. Nevertheless, a careful estimate of the RGB slope is a complicated task, even in the K, $(J-K)$ plane, where the RGB is steeper than

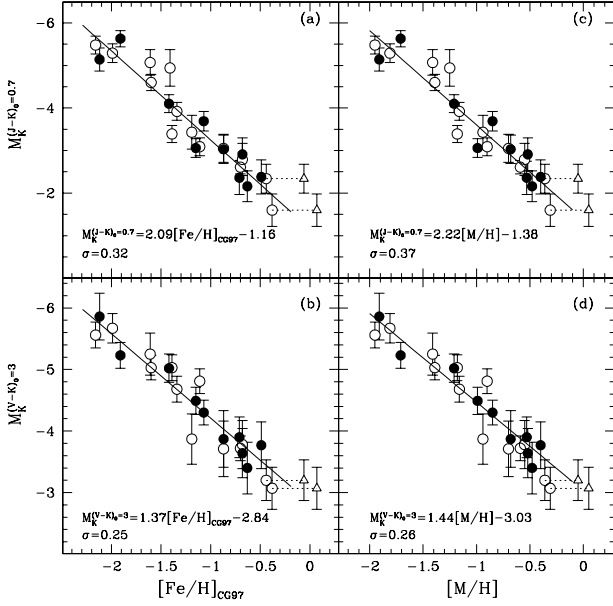


Figure 9. Upper panels: M_K at fixed $(J-K)_0 = 0.7$ as a function of the metallicity in the CG97 (a) and in the global (c) scale. Lower panels: M_K at constant $(V-K)_0 = 3$ as a function of the CG97 (b) and global (d) metallicity. The filled circles refer to the present sample, the empty circles mark the F00, V04 and S04 data and the empty triangles point NGC 6553 and NGC 6528 adopting the Carretta et al. (2001) metallicity estimates. The solid lines are best-fitting relations.

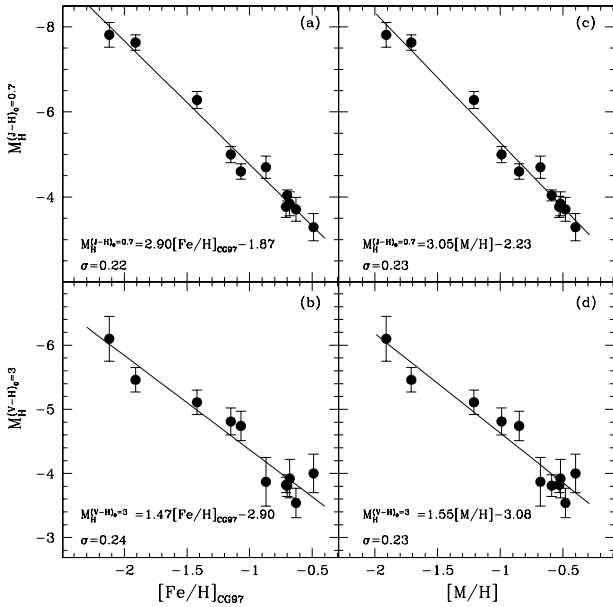


Figure 10. The same as Fig. 9, but for M_H magnitudes.

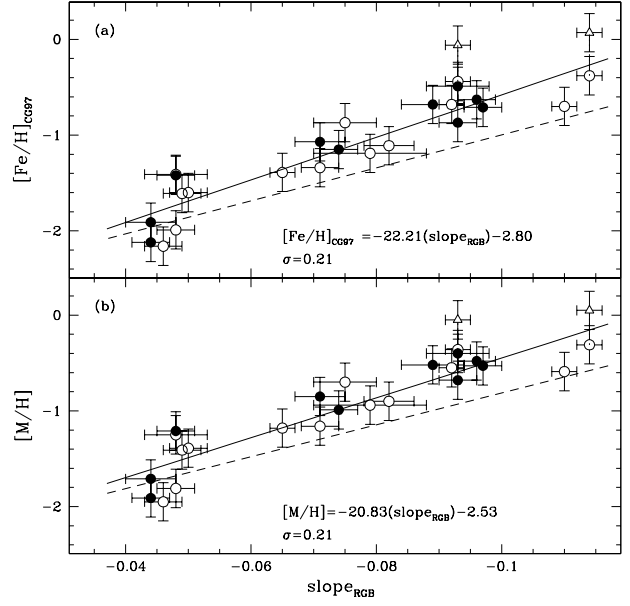


Figure 11. Metallicity scale: $[Fe/H]_{CG97}$ (a), and $[M/H]$ (b) as a function of the derived RGB slope for the selected 10 GCs (filled circles) and for the F00, V04 and S04 program clusters (empty circles). The solid lines are our best-fitting relations, while the dashed lines are the relations found by Ivanov & Borissova (2003).

in any other plane. As shown by Kuchinski et al. (1995); Kuchinski & Frogel (1995), a reasonable description of the overall RGB morphology can be obtained by linearly fitting the RGB in the range between 0.6 and 5.1 magnitudes brighter than the Zero Age Horizontal Branch (ZAHB). However, in the case of low-intermediate metallicity clusters the accurate measurement of the location of the ZAHB in the IR CMD is an almost impossible task, because the HB is not horizontal at all. In order to apply an homogeneous procedure to the entire cluster sample, we fit the RGB in a magnitude range between 0.5 and 5 magnitudes fainter than the brightest star of each cluster after a previous decontamination by the Asymptotic Giant Branch (AGB) and field stars. In particular, in the case of the Bulge clusters, the level of field contamination was estimated from the comparison with a *field*-CMD obtained from the 2MASS catalog for an equivalent area ($4' \times 4'$) located at $10'$ from the clusters center. On the basis of this comparison, a typical bulge contamination of 20% was found in the RGB region. Then the estimated number of field stars has been randomly removed from the cluster RGB sample, before determining the RGB slope. The derived RGB slope values for the entire sample are listed in Table 4. Fig. 11 shows the linear correlation of the RGB slope with the metallicity (in both the adopted scales); the inferred relations, with the corresponding standard deviations, are also reported in each panel. As expected the RGB slope becomes progressively steeper with decreasing metallicity, confirming the results found by Kuchinski et al. (1995); Kuchinski & Frogel (1995) and F00. The considerable disagreement between our results and the inferred relations found by Ivanov & Borissova (2003) (dashed lines in Fig. 11)

in particular in the high metallicity range, are mainly due to two different reasons: *i)* their sample of 22 GCs includes only 3 clusters more metal-rich than $[Fe/H]_{CG97} = -1$ and none more metallic than 47 Tuc, while our best-fitting relations are based on a global sample of 24 clusters, among them 7 more metal-rich than 47 Tuc, *ii)* the discrepancy in the estimate of the 47 Tuc RGB slope (-0.110 ± 0.002 , F00 and -0.125 ± 0.002 Ivanov & Borissova (2003)). Indeed, Ivanov & Borissova (2003) computed a weighed average relation which turned to be significantly influenced by the value of 47 Tuc, being the cluster with the most accurate determination.

5 SUMMARY AND CONCLUSIONS

A new set of high-quality IR CMDs for a sample of 10 GGCs spanning a wide metallicity range have been presented. This database has been combined with the data set collected by our group over the last 10 years (see F00, V04 and S04) and it has been used to measure a few major observables describing the main photometric properties of the RGB, namely: *i)* the location in colour and in magnitude, and *ii)* its slope. The behaviour of these quantities as a function of the clusters metallicity has been studied in both $[Fe/H]_{CG97}$ and $[M/H]$ metallicity scales. Since our database also include observations in the H-band, it has been used to derive for the first time the calibrations in the H, J-H and H, V-H planes, as well. All the relations are reported in the corresponding panels of Figs. 5-11 and in the Appendix, for more clarity.

ACKNOWLEDGMENTS

Part of the data analysis has been performed with the software developed by P. Montegriffo at the Osservatorio Astronomico di Bologna (INAF). This publication makes use of data products from the Two Micron All Sky Survey, which is a joint project of the University of Massachusetts and Infrared Processing and Analysis Center/California Institute of Technology, founded by the National Aeronautics and Space Administration and the National Science Foundation. The financial support by the Agenzia Spaziale Italiana (ASI) and the Ministero dell'Istruzione, Università e Ricerca (MIUR) is kindly acknowledged.

APPENDIX

In this appendix we report all the relations linking the photometric indices defined in the paper as a function of the cluster metallicity in both CG97 and global scale.

(J-K)₀ colours at fixed $M_K = (-5.5, -5, -4, -3)$ magnitudes:

$$(J - K)_0^{M_K = -5.5} = 0.22[Fe/H]_{CG97} + 1.14 \quad (1)$$

$$(J - K)_0^{M_K = -5} = 0.20[Fe/H]_{CG97} + 1.06 \quad (2)$$

$$(J - K)_0^{M_K = -4} = 0.16[Fe/H]_{CG97} + 0.93 \quad (3)$$

$$(J - K)_0^{M_K = -3} = 0.13[Fe/H]_{CG97} + 0.83 \quad (4)$$

$$(J - K)_0^{M_K = -5.5} = 0.23[M/H] + 1.11 \quad (5)$$

$$(J - K)_0^{M_K = -5} = 0.21[M/H] + 1.04 \quad (6)$$

$$(J - K)_0^{M_K = -4} = 0.17[M/H] + 0.92 \quad (7)$$

$$(J - K)_0^{M_K = -3} = 0.14[M/H] + 0.81 \quad (8)$$

(V-K)₀ colours at fixed $M_K = (-5.5, -5, -4, -3)$ magnitudes:

$$(V - K)_0^{M_K = -5.5} = 0.90[Fe/H]_{CG97}^2 + 3.30[Fe/H]_{CG97} + 5.98 \quad (9)$$

$$(V - K)_0^{M_K = -5} = 0.34[Fe/H]_{CG97}^2 + 1.50[Fe/H]_{CG97} + 4.49 \quad (10)$$

$$(V - K)_0^{M_K = -4} = 0.38[Fe/H]_{CG97} + 3.29 \quad (11)$$

$$(V - K)_0^{M_K = -3} = 0.26[Fe/H]_{CG97} + 2.87 \quad (12)$$

$$(V - K)_0^{M_K = -5.5} = 1.10[M/H]^2 + 3.52[M/H] + 5.77 \quad (13)$$

$$(V - K)_0^{M_K = -5} = 0.41[M/H]^2 + 1.60[M/H] + 4.37 \quad (14)$$

$$(V - K)_0^{M_K = -4} = 0.40[M/H] + 3.23 \quad (15)$$

$$(V - K)_0^{M_K = -3} = 0.28[M/H] + 2.83 \quad (16)$$

(J-H)₀ colours at fixed $M_H = (-5.5, -5, -4, -3)$ magnitudes:

$$(J - H)_0^{M_H = -5.5} = 0.20[Fe/H]_{CG97} + 0.97 \quad (17)$$

$$(J - H)_0^{M_H = -5} = 0.19[Fe/H]_{CG97} + 0.92 \quad (18)$$

$$(J - H)_0^{M_H = -4} = 0.16[Fe/H]_{CG97} + 0.82 \quad (19)$$

$$(J - H)_0^{M_H = -3} = 0.14[Fe/H]_{CG97} + 0.74 \quad (20)$$

$$(J - H)_0^{M_H = -5.5} = 0.21[M/H] + 0.94 \quad (21)$$

$$(J - H)_0^{M_H = -5} = 0.20[M/H] + 0.90 \quad (22)$$

$$(J - H)_0^{M_H = -4} = 0.17[M/H] + 0.80 \quad (23)$$

$$(J - H)_0^{M_H = -3} = 0.15[M/H] + 0.72 \quad (24)$$

(V-H)₀ colours at fixed $M_H = (-5.5, -5, -4, -3)$ magnitudes:

$$(V - H)_0^{M_H = -5.5} = 0.76[Fe/H]_{CG97}^2 + 2.81[Fe/H]_{CG97} + 5.50 \quad (25)$$

$$(V - H)_0^{M_H = -5} = 0.53[Fe/H]_{CG97}^2 + 2.08[Fe/H]_{CG97} + 4.77 \quad (26)$$

$$(V - H)_0^{M_H = -4} = 0.44[Fe/H]_{CG97} + 3.30 \quad (27)$$

$$(V - H)_0^{M_H = -3} = 0.36[Fe/H]_{CG97} + 2.92 \quad (28)$$

$$(V - H)_0^{M_H = -5.5} = 0.89[M/H]^2 + 2.89[M/H] + 5.23 \quad (29)$$

$$(V - H)_0^{M_H = -5} = 0.66[M/H]^2 + 2.22[M/H] + 4.61 \quad (30)$$

$$(V - H)_0^{M_H = -4} = 0.46[M/H] + 3.24 \quad (31)$$

$$(V - H)_0^{M_H = -3} = 0.37[M/H] + 2.87 \quad (32)$$

M_K magnitudes at fixed (J-K)₀ = 0.7 and (V-K)₀ = 3 colours:

$$M_K^{(J-K)_0 = 0.7} = 2.09[Fe/H]_{CG97} - 1.16 \quad (33)$$

$$M_K^{(V-K)_0 = 3} = 1.37[Fe/H]_{CG97} - 2.84 \quad (34)$$

$$M_K^{(J-K)_0 = 0.7} = 2.22[M/H] - 1.38 \quad (35)$$

Table 4. RGB location in colour (columns [4, 5, 6, 7]), in magnitude (column [8]) in the K, J-K plane and the RGB slope for the observed GCs and for the F00, V04 and S04 samples.

Name	$[Fe/H]_{CG97}$	$[M/H]$	$(J-K)_0^{-5.5}$	$(J-K)_0^{-5}$	$(J-K)_0^{-4}$	$(J-K)_0^{-3}$	$M_K^{(J-K)=0.7}$	RGB _{Slope}
M 15	-2.12	-1.91	0.725±0.025	0.690±0.023	0.629±0.022	0.577±0.020	-5.14±0.27	-0.044±0.003
M 30	-1.91	-1.71	0.689±0.016	0.653±0.014	0.597±0.012	0.558±0.011	-5.63±0.19	-0.044±0.004
NGC 6752	-1.42	-1.21	0.811±0.018	0.766±0.016	0.693±0.014	0.639±0.012	-4.10±0.21	-0.048±0.003
NGC 362	-1.15	-0.99	0.882±0.017	0.837±0.017	0.761±0.014	0.697±0.013	-3.06±0.22	-0.074±0.003
NGC 288	-1.07	-0.85	0.822±0.015	0.786±0.015	0.718±0.014	0.663±0.013	-3.69±0.23	-0.071±0.004
NGC 6380	-0.87	-0.68	0.954±0.052	0.895±0.052	0.789±0.051	0.697±0.050	-3.03±0.33	-0.094±0.003
NGC 6342	-0.71	-0.53	1.005±0.053	0.946±0.052	0.840±0.051	0.749±0.051	-2.36±0.39	-0.102±0.003
NGC 6441	-0.68	-0.52	0.958±0.053	0.898±0.052	0.792±0.051	0.707±0.050	-2.91±0.39	-0.092±0.005
NGC 6624	-0.63	-0.48	1.023±0.052	0.962±0.052	0.855±0.051	0.764±0.051	-2.16±0.36	-0.095±0.003
NGC 6440	-0.49	-0.40	1.020±0.053	0.957±0.052	0.847±0.051	0.753±0.051	-2.38±0.40	-0.093±0.005
M 68	-1.99	-1.81	0.712±0.013	0.683±0.013	0.629±0.012	0.582±0.012	-5.29±0.22	-0.048±0.003
M 55	-1.61	-1.41	0.735±0.023	0.694±0.023	0.629±0.021	0.578±0.021	-5.07±0.30	-0.049±0.003
M 4	-1.19	-0.94	0.864±0.028	0.821±0.027	0.741±0.027	0.671±0.026	-3.43±0.40	-0.079±0.009
M 107	-0.87	-0.70	0.966±0.031	0.903±0.031	0.790±0.029	0.696±0.027	-3.05±0.33	-0.075±0.005
47 Tuc	-0.70	-0.59	1.003±0.018	0.934±0.016	0.819±0.014	0.729±0.012	-2.61±0.16	-0.110±0.002
M 69	-0.68	-0.55	0.964±0.031	0.906±0.030	0.804±0.028	0.717±0.027	-2.79±0.38	-0.092±0.002
NGC 6553	-0.44	-0.36	1.036±0.052	0.971±0.053	0.852±0.052	0.753±0.051	-2.34±0.34	-0.092±0.002
NGC 6528	-0.38	-0.31	1.097±0.053	1.034±0.052	0.919±0.052	0.818±0.051	-1.60±0.38	-0.114±0.002
M 92	-2.16	-1.95	0.701±0.014	0.670±0.013	0.611±0.013	0.563±0.012	-5.48±0.21	-0.046±0.003
M 10	-1.41	-1.25	0.735±0.026	0.703±0.026	0.644±0.026	0.591±0.026	-4.94±0.43	-0.048±0.005
M 13	-1.39	-1.18	0.877±0.018	0.831±0.017	0.746±0.015	0.672±0.014	-3.39±0.20	-0.065±0.002
M 3	-1.34	-1.16	0.827±0.019	0.779±0.016	0.705±0.013	0.652±0.012	-3.92±0.21	-0.071±0.003
M 5	-1.11	-0.90	0.889±0.017	0.844±0.016	0.764±0.015	0.693±0.014	-3.09±0.21	-0.082±0.004
ω Cen	-1.60	-1.39	0.766±0.020	0.728±0.020	0.660±0.020	0.599±0.020	-4.602±0.19	-0.050±0.003

$$M_K^{(V-K)_0=3} = 1.44[M/H] - 3.03 \quad (36)$$

M_H magnitudes at fixed $(J-H)_0 = 0.7$ and $(V-H)_0 = 3$ colours:

$$M_H^{(J-H)_0=0.7} = 2.90[Fe/H]_{CG97} - 1.87 \quad (37)$$

$$M_H^{(V-H)_0=3} = 1.47[Fe/H]_{CG97} - 2.90 \quad (38)$$

$$M_H^{(J-H)_0=0.7} = 3.05[M/H] - 2.23 \quad (39)$$

$$M_H^{(V-H)_0=3} = 1.55[M/H] - 3.08 \quad (40)$$

The RGB slope:

$$[Fe/H]_{CG97} = -22.21(slope_{RGB}) - 2.80 \quad (41)$$

$$[M/H] = -20.83(slope_{RGB}) - 2.53 \quad (42)$$

REFERENCES

- Bellazzini, M., Fusi Pecci, F., Ferraro, F. R., Galletti, S., Catelan, M. & Landsman, W. B. 2001, AJ, 122,2569
- Bergbusch, P. A. 1996, AJ, 112,1061
- Buonanno, R., Corsi, C. E. & Fusi Pecci, F. 1985, A&A, 145,97
- Carretta, E. & Gratton, R. G. 1997, A&AS, 121, 95 (CG97)
- Carretta, E., Cohen, J. G. & Gratton, R. G. 2001, AJ, 122,1469
- Cohen, J. G. & Sleeper, C. 1995, AJ, 109,242
- Davidge, T. J. & Harris, W. E. 1997, AJ, 475,584
- Feltzing, S. & Johnson, R. A. 2002, A&A, 385,67
- Ferraro, F. R., Fusi Pecci, F., Guarneri, M. D., Moneti, A., Origlia, L. & Testa, V. 1994, MNRAS, 266, 829
- Ferraro, F. R., Messineo, Fusi Pecci, F., De Palo, M. A., Straniero, O., Chieffi, A. & Limongi, M. 1999, AJ, 118, 1738 (F99)
- Ferraro, F. R., Montegriffo, P., Origlia, L., & Fusi Pecci, F. 2000, AJ, 119, 1282, (F00)
- Ferraro, F. R., Possenti, A., Sabbi, E., Lagani, P., Rood, R. T., D'Amico, N. & Origlia, L. 2003, ApJ, 595,179
- Frogel, J. A., Cohen, J. G. & Persson, S. E. 1983, ApJ, 275,773
- Frogel, J. A., Persson, S. E. & Cohen, J. G. 1983, ApJS, 53,713
- Harris, W. E. 1996, AJ, 112,1487
- Heasley, J. N., Janes, K. A., Zinn, R., Demarque, P., Da Costa, G. S. & Christian, C. A. 2000, AJ, 120,879
- Ivanov, V. D. & Borissova, J. 2002, A&A, 390,973
- Kuchinski, L. E. & Frogel, J. A. 1995, AJ, 110,284
- Kuchinski, L. E., Frogel, J. A., Terndrup, D. M. & Persson, S. E. 1995, AJ, 109,1131

Table 5. RGB $(V-K)_0$ colours at fixed magnitudes ($M_K = -5.5, -5, -4, -3$) and K absolute magnitude at constant $(V-K)_0$ colour for the observed GCs and for the F00, V04 and S04 samples.

Name	$[Fe/H]_{CG97}$	$[M/H]$	$(V-K)_0^{-5.5}$	$(V-K)_0^{-5}$	$(V-K)_0^{-4}$	$(V-K)_0^{-3}$	$M_K^{(V-K)_0=3}$
M 15	-2.12	-1.91	2.886±0.118	2.743±0.116	2.505±0.113	2.315±0.112	-5.86±0.38
M 30	-1.91	-1.71	3.106±0.083	2.914±0.077	2.611±0.067	2.392±0.062	-5.23±0.21
NGC 6752	-1.42	-1.21	3.157±0.074	2.993±0.072	2.696±0.068	2.441±0.064	-5.02±0.23
NGC 362	-1.15	-0.99	3.389±0.083	3.189±0.080	2.831±0.075	2.532±0.068	-4.49±0.22
NGC 288	-1.07	-0.85	3.504±0.089	3.280±0.085	2.889±0.076	2.569±0.069	-4.30±0.20
NGC 6380	-0.87	-0.68	3.938±0.294	3.601±0.288	3.051±0.291	2.703±0.276	-3.87±0.46
NGC 6342	-0.71	-0.53	4.078±0.301	3.681±0.295	3.049±0.284	2.635±0.276	-3.90±0.33
NGC 6441	-0.68	-0.52	4.167±0.331	3.674±0.302	3.132±0.278	2.770±0.277	-3.64±0.40
NGC 6624	-0.63	-0.48	3.985±0.308	3.622±0.288	3.204±0.278	2.875±0.276	-3.40±0.42
NGC 6440	-0.49	-0.40	4.380±0.337	3.827±0.311	3.113±0.284	2.754±0.275	-3.77±0.38
M 68	-1.99	-1.81	2.949±0.070	2.808±0.067	2.562±0.064	2.360±0.061	-5.67±0.24
M 55	-1.61	-1.41	3.094±0.124	2.910±0.121	2.609±0.116	2.379±0.113	-5.25±0.34
M 4	-1.19	-0.94	—	3.464±0.152	3.049±0.148	2.706±0.144	-3.87±0.41
M 107	-0.87	-0.70	3.798±0.161	3.535±0.155	3.105±0.147	2.780±0.142	-3.71±0.45
47 Tuc	-0.70	-0.59	3.900±0.099	3.559±0.081	3.098±0.066	2.792±0.060	-3.72±0.20
M 69	-0.68	-0.55	3.830±0.161	3.559±0.157	3.094±0.150	2.723±0.145	-3.86±0.33
NGC 6553	-0.44	-0.36	5.023±0.346	4.396±0.323	3.480±0.294	2.904±0.281	-3.20±0.33
NGC 6528	-0.38	-0.31	5.255±0.365	4.553±0.334	3.561±0.298	2.968±0.281	-3.07±0.34
M 92	-2.16	-1.95	2.978±0.078	2.808±0.073	2.538±0.065	2.342±0.060	-5.56±0.21
M 13	-1.39	-1.18	3.189±0.086	2.987±0.079	2.661±0.069	2.421±0.063	-5.03±0.21
M 3	-1.34	-1.16	3.355±0.092	3.126±0.086	2.768±0.071	2.514±0.063	-4.68±0.21
M 5	-1.11	-0.90	3.310±0.092	3.079±0.085	2.694±0.076	2.380±0.070	-4.81±0.20
ω Cen	-1.60	-1.39	3.202±0.030	2.988±0.030	2.648±0.030	2.402±0.030	-5.03±0.20

Table 6. RGB $(J-H)_0$ colours at fixed magnitudes ($M_H = -5.5, -5, -4, -3$) and H absolute magnitude at constant $(J-H)_0$ for the observed GCs.

Name	$[Fe/H]_{CG97}$	$[M/H]$	$(J-H)_0^{-5.5}$	$(J-H)_0^{-5}$	$(J-H)_0^{-4}$	$(J-H)_0^{-3}$	$M_H^{(J-H)_0=0.7}$
M 15	-2.12	-1.91	0.579±0.02	0.554±0.02	0.512±0.02	0.476±0.01	-7.81±0.29
M 30	-1.91	-1.71	0.563±0.01	0.533±0.01	0.484±0.01	0.447±0.01	-7.63±0.18
NGC 6752	-1.42	-1.21	0.658±0.01	0.630±0.01	0.579±0.01	0.534±0.01	-6.28±0.20
NGC 362	-1.15	-0.99	0.734±0.01	0.700±0.01	0.639±0.01	0.585±0.01	-5.00±0.19
NGC 288	-1.07	-0.85	0.759±0.01	0.729±0.01	0.660±0.01	0.598±0.01	-4.60±0.18
NGC 6380	-0.87	-0.68	0.762±0.04	0.722±0.04	0.649±0.04	0.585±0.03	-4.70±0.26
47 Tuc	-0.70	-0.59	0.821±0.02	0.777±0.01	0.697±0.01	0.628±0.01	-4.04±0.13
NGC 6342	-0.71	-0.53	0.856±0.04	0.807±0.04	0.719±0.04	0.644±0.04	-3.77±0.25
NGC 6441	-0.68	-0.52	0.841±0.04	0.794±0.04	0.713±0.04	0.646±0.03	-3.84±0.28
NGC 6624	-0.63	-0.48	0.839±0.04	0.797±0.04	0.730±0.04	0.657±0.03	-3.71±0.28
NGC 6440	-0.49	-0.40	0.867±0.04	0.823±0.04	0.746±0.04	0.683±0.03	-3.29±0.32

Table 7. RGB $(V-H)_0$ colours at fixed magnitudes ($M_H=-5.5, -5, -4, -3$) and H absolute magnitude at constant $(V-H)_0$ colour for the observed GCs.

Name	$[Fe/H]_{CG97}$	$[M/H]$	$(V-H)_0^{-5.5}$	$(V-H)_0^{-5}$	$(V-H)_0^{-4}$	$(V-H)_0^{-3}$	$M_H^{(V-H)_0=3}$
M 15	-2.12	-1.91	2.815±0.11	2.674±0.11	2.430±0.11	2.224±0.11	-6.10±0.35
M 30	-1.91	-1.71	3.019±0.09	2.814±0.08	2.495±0.07	2.274±0.06	-5.46±0.19
NGC 6752	-1.42	-1.21	3.169±0.09	2.952±0.08	2.592±0.07	2.319±0.06	-5.11±0.19
NGC 362	-1.15	-0.99	3.246±0.08	3.065±0.07	2.737±0.07	2.451±0.07	-4.81±0.21
NGC 288	-1.07	-0.85	3.242±0.07	3.080±0.07	2.785±0.07	2.520±0.06	-4.74±0.23
NGC 6380	-0.87	-0.68	3.880±0.28	3.547±0.27	3.047±0.27	2.717±0.26	-3.87±0.38
47 Tuc	-0.70	-0.59	4.012±0.10	3.630±0.09	3.080±0.07	2.736±0.06	-3.81±0.17
NGC 6342	-0.71	-0.53	3.975±0.28	3.641±0.27	3.082±0.27	2.659±0.26	-3.82±0.12
NGC 6441	-0.68	-0.52	4.175±0.31	3.720±0.27	3.043±0.27	2.624±0.26	-3.92±0.30
NGC 6624	-0.63	-0.48	4.177±0.28	3.810±0.28	3.216±0.27	2.785±0.26	-3.54±0.23
NGC 6440	-0.49	-0.40	4.186±0.31	3.683±0.29	3.001±0.27	2.647±0.26	-4.00±0.30

- Melndez, J., Barbuy, B., Bica, E., Zoccali, M., Ortolani, S., Renzini, A. & Hill, V. 2003, A&A, 411, 417
- Minniti, D., Olszewski, W. E. & Rieke, M. 1995, AJ, 110,1686
- Momany, Y., Ortolani, S., Held, E. V., Barbuy, B., Bica, E., Renzini, A., Bedin, L. R., Rich, R. M. & Marconi, G. 2003, A&A, 402,607
- Montegriffo, P., Ferraro, F. R., Fusi Pecci, F., & Origlia, L. 1995 MNRAS, 276, 739
- Moorwood et al. 1992, The Messenger, 69,61
- Origlia, L., Rich, R. M., & Castro S. 2002, AJ, 123,1559
- Origlia, L. & Rich, R. M. 2004, in prep.
- Ortolani, S., Bica, E. & Barbuy, B 1994, A&AS, 108,653
- Ortolani, S., Bica, E. & Barbuy, B 1998, A&AS, 127,471
- Ortolani, S., Barbuy, B., Bica, E., Renzini, A., Zoccali, M., Rich, R. M. & Cassisi, S. 2001, A&A, 376,878
- Piotto, G., King, I. R., Djorgovski, S. G., Sosin, D., Zoccali, M., Saviane, I., De Angeli, F., Riello, M., Recio Blanco, A., Rich, R. M., Meylan, G. & Renzini, A. 2002 A&A, 391,945
- Renzini, A. & Fusi Pecci, F. 1988, ARA&A,26,199
- Rich, R. M. et al. 1997, ApJ, 484,25
- Savage, B. D. & Mathis, J. S. 1979, ARA&A, 17, 73
- Schlegel, D. J., Finkbeiner, D. P. & Davis, M. 1998, ApJ, 500,525
- Sollima, A., Ferraro, F. R., Origlia, L., Pancino, E. & Bellazzini, M. 2004, A&A submitted
- Stetson, P. B. & Harris, W. E. 1988, AJ, 96,909
- Stetson, P. B. 1987, PASP,99,191
- Straniero, O., Chieffi, A. & Limongi, M. 1997, ApJ, 490,425 (SCL97)
- Valenti, E., Ferraro, F. R., Perina, S. & Origlia, L. 2004, A&A, astro-ph/0401153
- Zinn, R. 1985, ApJ,293,424